JACS
JOURNAL OF THE AMERICAN CHEMICAL SOCIETY

Communication

pubs.acs.org/JACS

Catalytic Mesoporous Janus Nanomotors for Active Cargo Delivery

Xing Ma,[†] Kersten Hahn,[†] and Samuel Sanchez*[,†,‡,§]

[†]Max Planck Institute for Intelligent Systems Institution, Heisenbergstraße 3, 70569 Stuttgart, Germany

[‡]Institució Catalana de Recerca i EstudisAvancats (ICREA), Pg. Lluís Companys 23, 08010, Barcelona, Spain

[§]Institut de Bioenginyeria de Catalunya (IBEC), Baldiri i Reixac 10-12, 08028 Barcelona, Spain

Supporting Information

ABSTRACT: We report on the synergy between catalytic propulsion and mesoporous silica nanoparticles (MSNPs) for the design of Janus nanomotors as active cargo delivery systems with sizes <100 nm (40, 65, and 90 nm). The Janus asymmetry of the nanomotors is given by electron beam (e-beam) deposition of a very thin platinum (2 nm) layer on MSNPs. The chemically powered Janus nanomotors present active diffusion at low H_2O_2 fuel concentration (i.e., <3 wt %). Their apparent diffusion coefficient is enhanced up to 100% compared to their Brownian motion. Due to their mesoporous architecture and small dimensions, they can load cargo molecules in large quantity and serve as active nanocarriers for directed cargo delivery on a chip.

Since pioneering contributions by the research groups from Penn State[1] and Toronto[2] 10 years ago, chemically driven self-propelled micro-/nanomotors (MNMs) have been extensively developed and designed to accomplish various tasks in fluids.[3−10] Scientists have designed artificial swimmers similar in scale to enzymes,[11] virus,[12−15] and motile cells[16−22] that use self-propulsion mechanisms to overcome Brownian forces that nano- and microswimmers experience in fluids. As the size-scale reduces, the effect of viscosity increases making the motion of nanomotors at low Reynolds numbers challenging.[23] However, unique physicochemical properties and novel functions of nanoparticles, especially those <100 nm, have attracted considerable attention.[24] Therefore, either from the view of fundamental scientific exploration or under the guidance of practical applications, it is of great significance to develop self-powered motors at the nanoscale, which can lead to a hybrid nanoplatform by combining the smart motion of nanomotors with the special characteristics of nanoparticles.

Cargo transport is a hot research topic of MNMs.[25−28] Especially, nanomotors capable of both autonomous motion and cargo delivery at small scales may lead to promising novel active nanocarriers with potential biomedical relevance. Compared to previous passive cargo delivery nanosystems, self-propelled nanomotors might be able to actively deliver cargos to the targeted site as required, provided the utilization of proper guidance methods such as chemotaxis,[29−32] pH taxis,[33] phototaxis[34] or remote magnetic guidance.[26] In order to fabricate autonomous nanosystems with large cargo loading capabilities, mesoporous silica nanoparticles (MSNPs) are an ideal candidate for that purpose. MSNPs were initially invented by two independent research groups,[35,36] and since then this new type of nanoparticles has been widely investigated and developed for different applications, by virtue of its unique mesoporous structure and tunable particle size.[37−39] The mesopores can ensure much higher cargo loading capacity compared to solid nanoparticles because of their extremely high specific surface area (>1000 m^2/g) and pore volume (>1 cm^3/g).[40−42] Recent reports have demonstrated that chemically powered asymmetric particles are excellent platforms for mimicking the motion of biological nanoswimmers, as they can move by phoretic mechanisms where the propulsion forces are generated on-board, i.e. self-diffusiophoresis[19,43,44] or self-electrophoresis.[20,45,46] However, the use of Janus mesoporous nanomotors for catalytic propulsion, together with cargo loading and release capabilities, in desired locations has been rarely explored.

Here, we present Janus nanomotors based on MSNPs with tunable size within 100 nm (40, 65, 90 nm) and carried out comprehensive characterization on the nanomotors' morphology and structure. Noteworthy, we performed a systematic study on their self-propulsion in dilute hydrogen peroxide solutions using dynamic light scattering (DLS) and optical imaging. In addition, we present their feasibility as potential active nanocarriers for cargo delivery. The fabrication strategy is presented in Scheme S1 in the Supporting Information (SI). The platinum catalytic layer triggers the decomposition of H_2O_2 to produce the driving force by self-diffusiophoresis within self-generated chemical gradients. Small cargo molecules can be loaded into the mesopores at the noncoated side of the Janus nanomotors and delivered to target locations on a chip by using specially designed walls.

The MSNPs of different sizes were first synthesized via a classic "sol-gel" process, using silica precursor tetraethylorthosilicate (TEOS) and surfactant molecule cetyltrimethylammonoium bromide (CTAB) in aqueous solution. In order to obtain monodispersed MSNPs without aggregations, a weak base triethanolamine (TEOA) has been used as the catalyst.[47,48] Briefly, MSNP(40 nm) and MSNP(65 nm) were directly synthesized by a one-step method according to previous reports with minor modifications,[49] while MSNP(90 nm) were synthesized by a two-step seed-growth method[50] (see detailed procedure in the SI). The MSNPs of 40, 65, and 90 nm were completely monodispersed, as shown by scanning electron microscopy (SEM) images in Figures S1a−f and S2. Inset images in Figure S1d−f indicate the nanosized mesopores (2−3 nm).

Received: March 17, 2015
Published: April 6, 2015

DOI: 10.1021/jacs.5b02700
J. Am. Chem. Soc. 2015, 137, 4976−4979

Janus mesoporous silica nanomotors (JMSNMs) were fabricated by depositing a thin layer (2 nm) of Pt onto the MSNPs monolayers by electron-beam (e-beam) evaporation at zero degree, leading to two different faces of each side of the nanoparticles. Hence, the mesopores at the noncoated side of the JMSNM are still accessible to small molecules, for cargo loading. Transmission electron microscopy (TEM) bright-field (BF) images in Figure 1a show JMSNM of different sizes with Pt

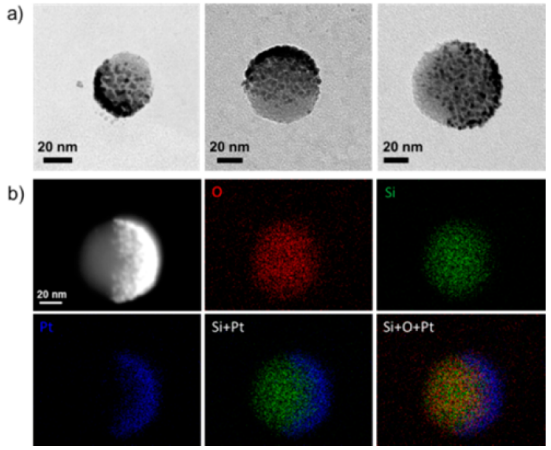

Figure 1. Characterization of Janus mesoporous nanomotors. (a) TEM-BF images of JMSNM(40 nm)-Pt(2 nm), JMSNM(65 nm)-Pt(2 nm), and JMSNM(90 nm)-Pt(2 nm), from left to right, respectively. (b) STEM-HAADF image and element mapping of JMSNM(65 nm)-Pt(2 nm) by EDX.

coating layers as a dark color. Due to the ultrathin layer deposition, instead of forming a uniform and continuous smooth coating layer, the catalytic layers form Pt islands which were reported to exhibit better catalytic performance than smooth ones.[51,52] JMSNM(65 nm)-Pt(2 nm) was chosen for element mapping by scanning transmission electron microscopy (STEM) high-angle annular dark field (HAADF) and energy-dispersive X-ray spectroscopy (EDX) (Figure 1b). Corresponding EDX spectra of the Pt coated and noncoated sides were both acquired (Figure S3 in the SI). The Janus structure was clearly outlined by the element mapping, as both oxygen (O: red) and silicon (Si: green) elements show a spherical shape while the Pt (blue) element covers one-half of a sphere.

Dynamic light scattering (DLS) was used to measure the apparent diffusion coefficient of the JMSNM. As illustrated in Figure 2a, the Pt layer at one side triggers the decomposition of H_2O_2 into O_2 and H_2O. The propulsion force of JMSNM is mainly attributed to a self-diffusiophoresis mechanism, where a chemical gradient is asymmetrically generated on both sides by catalytic reactions.[7,26,43,53] Upon increasing H_2O_2 fuel concentration, the apparent diffusion coefficient of JMSNM for the three sizes presents a growing trend and reaches a saturation plateau at a H_2O_2 concentration of ~2.5% wt (Figure 2b). For JMSNM(90 nm)and JMSNM(65 nm), the diffusion coefficient value was enhanced by nearly 100%.

Even for the ultrasmall JMSNM(40 nm) which has the strongest Brownian motion among the three sizes, the enhancement was as high as 50%. These data were confirmed by a clear right shift in the diffusion coefficient distribution curves (Figure S4 in the SI). A similar increase was recently reported by Fischer et al. on self-electrophoretic bimetallic nanomotors.[11] Without any H_2O_2, the different JMSNMs present different

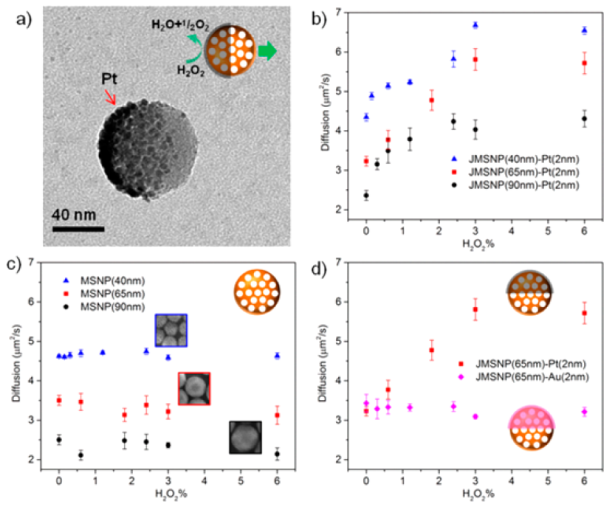

Figure 2. Dynamics of catalytic JMSNMs by DLS measurements. (a) TEM-BF image of JMSNM(65 nm) and schematic illustration (inset) of catalytic reaction providing self-propulsion. Apparent diffusion coefficient of (b) JMSNMs-Pt(2 nm), (c) MSNPs, and (d) comparison between JMSNM(65 nm)-Au(2 nm) and JMSNM(65 nm)-Pt(2 nm), with increasing H_2O_2 concentration.

diffusion coefficient values, according to the size dependence of the Brownian motion given by the classic Stokes−Einstein relation. The apparent diffusion coefficient measured by DLS is usually lower than the theoretical values, as DLS determines the particle's hydrodynamic size which is inherently larger than the particle's actual size. The presence of minor aggregations will also lead to a decrease in the apparent diffusion coefficient.

Diffusion of bare MSNPs showed no enhancement with increasing H_2O_2 concentration (0−6%) (Figure 2c), and no right shift was observed in the diffusion coefficient distribution curves (Figure S5a−c in the SI). To further prove the catalytic activity of the Pt layer, a JMSNP with similar weight and composition was fabricated as a negative control, by depositing catalytically inert element gold (Au) onto MSNP(65 nm) (Figure S6 in the SI). As expected, the apparent diffusion coefficient of JMSNP(65 nm)-Au(2 nm) did not increase (Figure 2d) and no right shift in the diffusion coefficient distribution curves was observed (Figure S5d in the SI). Furthermore, to confirm the self-propelling phenomenon of JMSNM, the diffusion activity of the JMSNM was directly observed by optical microscopy. JMSNM(90 nm) was chosen for microscopy observation because of the challenge to trace smaller nanoparticles in a reliable manner by optical microscopy. The trajectory of JMSNM was tracked by software ImageJ and plotted in Figure 3a. The movement of the nanomotors exhibited a typical "random walk". However, with the presence of H_2O_2, the area covered by the nanomotors' "walk path" is much larger than without H_2O_2 (i.e., Brownian motion), suggesting enhanced diffusion of the JMSNM (Figure 3a, videos S1 and S2 in the SI).

According to the definition of the diffusion coefficient (D), $D = \mathrm{MSD}/i{\cdot}\Delta t$, where MSD is the mean square displacement (MSD), Δt is the time interval, and i is the dimensional index. Here, for the case of two-dimensional analysis from the recorded videos, i is equal to 4 and $\mathrm{MSD} = (x(\Delta t) - x(0))^2 + (y(\Delta t) - y(0))^2$. The plots of MSD versus Δt were presented in Figure 3b. By linearly fitting their slopes, the diffusion coefficient can be calculated, and the results are shown in Figure 3c. The diffusion coefficient of the Brownian motion (without H_2O_2) calculated

DOI: 10.1021/jacs.5b02700
J. Am. Chem. Soc. 2015, 137, 4976−4979

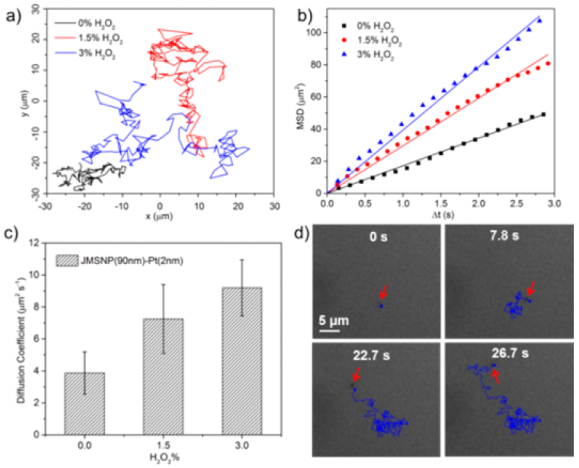

Figure 3. Optical video analysis on catalytic nanomotor of JMSNP(90 nm)-Pt(2 nm). (a) Trajectory tracking of the catalytic JMSNM with different H_2O_2 concentrations up to 30 s, (b) fitting plots of mean square displacement (MSD) versus time interval (Δt), analyzed from the trajectory tracking in (a), (c) apparent diffusion coefficient values, determined by equation MSD = $4 \cdot D \cdot \Delta t$, and (d) optical video snapshots extracted from optical videos in the SI of the JMSNM with 3% H_2O_2.

from the recorded video was 3.87 ± 1.32 $\mu m^2/s$ which is experimentally reasonable when compared to the theoretical value of nanoparticles with a 90 nm size, i.e. 4.77 $\mu m^2/s$. With addition of H_2O_2, this value was increased to 7.24 ± 2.15 $\mu m^2/s$ for 1.5% H_2O_2 and 9.20 ± 1.75 $\mu m^2/s$ for 3% H_2O_2. The enhancement was consistent with the results from DLS measurement. Typical video snapshots (30 fps) are shown in Figure 3d. Blue lines indicate the diffusion path of the Janus nanomotors noted by red arrows (video S2b in the SI).

Mesoporous material based nanomotors are of significant interest because of their high porosity for cargo loading. To evaluate that capability, first fluorescein isothiocyanate (FITC), a green fluorescence dye, was used to label MSNP(65 nm) by covalent linkage (see the detailed procedure in the Experimental Section in the SI) and then fabricate Janus nanomotors by further e-beam deposition, denoted as JMSNM(65 nm)@FITC-Pt. As illustrated in Figure 4a, the Rhodamine B (RhB) molecule was chosen as the model drug with red fluorescence color. By stirring

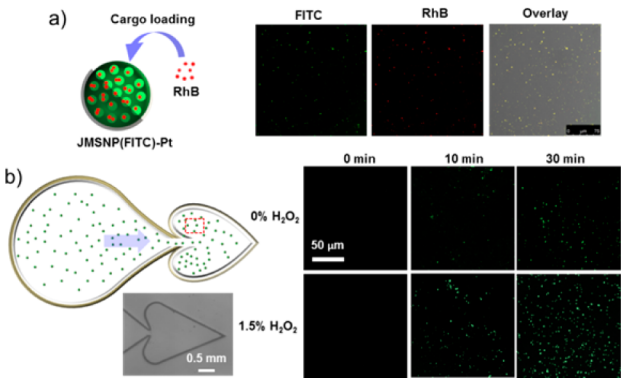

Figure 4. (a) Schematic illustration (left) and CLSM images of RhB loaded JMSNM(65 nm)@FITC-Pt, from left to right, are FITC channel, RhB channel, and overlay of bright field, FITC and RhB channels (scale bar is 75 μm). (b) Schematic illustration of on-chip cargo delivery by JMSNM, and CLSM images of active diffused JMSNM taken after 0, 10, and 30 min from the location represented by the red box in the scheme.

the JMSNM(65 nm)@FITC-Pt in concentrated RhB aqueous solution for 24 h, RhB cargo molecules were loaded into the mesopores of the nanomotors via free diffusion. Then, RhB loaded JMSNP(65 nm)@FITC-Pt were observed by confocal laser scanning microscopy (CLSM). The green dots indicate the location of the JMSNP(65 nm)@FITC-Pt, overlapped with the red dots, suggesting the RhB cargo molecules were indeed loaded inside the JMSNP(65 nm)@FITC-Pt (Figure 4a). A microchip comprised of two reservoirs that were connected by a channel with a width of 100 μm was used for the active cargo transport investigation.

In previous reports, tubular micromotors were trapped by physical boundaries due to a ratchet mechanism, using heart-shaped structures.[15,54] The RhB loaded nanomotors were initially placed in the left-side reservoir and then started to actively move into the small target chamber. The presence of cargo loaded nanomotors in the target chamber was monitored by CLSM at a region of interest (red box shown in the schematic from Figure 4b). With the presence of H_2O_2 fuel, many more transferred nanomotors were observed in the desired location compared to that without H_2O_2 fuel, based on the amount of fluorescent signal from the CLSM snapshots. This accumulation can be explained by the active diffusion of the nanomotors toward the target reservoir and the ratchet shape of the microchip without the use of external fields for guidance.

In order to investigate the cargo release, two different cargo molecules, RhB and methylene blue (MB), were loaded into JMSNM(65 nm)-Pt which were suspended into aqueous solution with and without H_2O_2. The release profile of RhB and MB was monitored by measuring the absorption intensity at 550 and 665 nm, respectively, at defined time intervals. Continuous release of RhB and MB from the JMSNM@FITC(65 nm)-Pt was observed for up to 8 h (Figure S7). Furthermore, the presence of H_2O_2 does not significantly affect the sustained release which is very useful for small cargo loading and delivery.[41,42,55,56] Solid silica nanomotors were used as a control for the release experiment (pink lines in Figure S7). Under the same conditions, the release profile remained at very low adsorption intensity, indicating the much lower loading capability of rigid spheres when compared to the mesoporous counterparts.

In conclusion, MSNP based Janus nanomotors with a tunable size of <100 nm were fabricated. DLS results and MSD analysis from optical videos revealed the enhanced diffusion of the JMSNM, indicating the self-propelling property of the nanomotors under strong Brownian motion. Furthermore, the synergy of autonomous motion and cargo loading capabilities at small scales may lead to promising novel active nanocarriers for small cargo delivery. In addition to the "smart walls concept" used in this work, other guiding approaches such as chemotaxis, pH taxis, or thermotaxis will be helpful to realize motion control for directed cargo transport to target locations. Although sustained release was observed in our work, further functionalization of "gate keepers", e.g. supramolecular host−guest complexes, at orifices of the mesopores will be able to realize external stimulus responsive cargo release at the target chamber only.[57−59]

■ ASSOCIATED CONTENT

Ⓢ Supporting Information

Experimental details, SEM and STEM characterization of MSNPs, DLS data, sustained cargo release plots, and videos.

DOI: 10.1021/jacs.5b02700
J. Am. Chem. Soc. 2015, 137, 4976−4979

This material is available free of charge via the Internet at http://pubs.acs.org.

AUTHOR INFORMATION

Corresponding Author

*sanchez@is.mpg.de, ssanchez@ibecbarcelona.eu

Notes

The authors declare no competing financial interest.

ACKNOWLEDGMENTS

Authors thank P. Fischer and M. Alarcón-Correa for instrument support and scientific discussions. The research leading to these results received funding from the European Union Seventh Framework Program [FP/2007/2013] under Grant Agreement No. 312483 (ESTEEM2), European Research Council under the European Union's Seventh Framework Program (FP7/2007/2013)/ERC Grant Agreement No. 311529 (LT-NRBS), and the Alexander von Humboldt Foundation.

REFERENCES

(1) Paxton, W. F.; Kistler, K. C.; Olmeda, C. C.; Sen, A.; St. Angelo, S. K.; Cao, Y. Y.; Mallouk, T. E.; Lammert, P. E.; Crespi, V. H. *J. Am. Chem. Soc.* **2004**, *126*, 13424.

(2) Fournier-Bidoz, S.; Arsenault, A. C.; Manners, I.; Ozin, G. A. *Chem. Commun.* **2005**, 441.

(3) Gaspar, S. *Nanoscale* **2014**, *6*, 7757.

(4) Wang, J. *Nanomachines: Fundamentals and Applications*; Wiley: 2013.

(5) Sengupta, S.; Ibele, M. E.; Sen, A. *Angew. Chem., Int. Ed.* **2012**, *51*, 8434.

(6) Wang, J. *ACS Nano* **2009**, *3*, 4.

(7) Wang, W.; Duan, W. T.; Ahmed, S.; Mallouk, T. E.; Sen, A. *Nano Today* **2013**, *8*, 531.

(8) Sánchez, S.; Soler, L.; Katuri, J. *Angew. Chem., Int. Ed.* **2015**, *54*, 1414.

(9) Gao, W.; Wang, J. *ACS Nano* **2014**, *8*, 3170.

(10) Guix, M.; Mayorga-Martinez, C. C.; Merkoci, A. *Chem. Rev.* **2014**, *114*, 6285.

(11) Lee, T.-C.; Alarcón-Correa, M.; Miksch, C.; Hahn, K.; Gibbs, J. G.; Fischer, P. *Nano Lett.* **2014**, *14*, 2407.

(12) Wilson, D. A.; Nolte, R. J. M.; van Hest, J. C. M. *Nat. Chem.* **2012**, *4*, 268.

(13) Xuan, M.; Shao, J.; Lin, X.; Dai, L.; He, Q. *ChemPhysChem* **2014**, *15*, 2255.

(14) Schamel, D.; Mark, A. G.; Gibbs, J. G.; Miksch, C.; Morozov, K. I.; Leshansky, A. M.; Fischer, P. *ACS Nano* **2014**, *8*, 8794.

(15) Gibbs, J. G.; Mark, A. G.; Lee, T.-C.; Eslami, S.; Schamel, D.; Fischer, P. *Nanoscale* **2014**, *6*, 9457.

(16) Tottori, S.; Zhang, L.; Peyer, K. E.; Nelson, B. J. *Nano Lett.* **2013**, *13*, 4263.

(17) Gao, W.; Sattayasamitsathit, S.; Orozco, J.; Wang, J. *J. Am. Chem. Soc.* **2011**, *133*, 11862.

(18) Zhao, G. J.; Ambrosi, A.; Pumera, M. *Nanoscale* **2013**, *5*, 1319.

(19) Baraban, L.; Tasinkevych, M.; Popescu, M. N.; Sanchez, S.; Dietrich, S.; Schmidt, O. G. *Soft Matter* **2012**, *8*, 48.

(20) Wang, Y.; Hernandez, R. M.; Bartlett, D. J., Jr.; Bingham, J. M.; Kline, T. R.; Sen, A.; Mallouk, T. E. *Langmuir* **2006**, *22*, 10451.

(21) Solovev, A. A.; Mei, Y. F.; Urena, E. B.; Huang, G. S.; Schmidt, O. G. *Small* **2009**, *5*, 1688.

(22) Howse, J. R.; Jones, R. A.; Ryan, A. J.; Gough, T.; Vafabakhsh, R.; Golestanian, R. *Phys. Rev. Lett.* **2007**, *99*, 048102.

(23) Purcell, E. M. *Am. J. Phys.* **1977**, *45*, 3.

(24) Kim, B. H.; Hackett, M. J.; Park, J.; Hyeon, T. *Chem. Mater.* **2014**, *26*, 59.

(25) Gao, W.; Wang, J. *Nanoscale* **2014**, *6*, 10486.

(26) Baraban, L.; Makarov, D.; Streubel, R.; Monch, I.; Grimm, D.; Sanchez, S.; Schmidt, O. G. *ACS Nano* **2012**, *6*, 3383.

(27) Wu, Z.; Wu, Y.; He, W.; Lin, X.; Sun, J.; He, Q. *Angew. Chem., Int. Ed.* **2013**, *52*, 7000.

(28) Patra, D.; Sengupta, S.; Duan, W. T.; Zhang, H.; Pavlick, R.; Sen, A. *Nanoscale* **2013**, *5*, 1273.

(29) Baraban, L.; Harazim, S. M.; Sanchez, S.; Schmidt, O. G. *Angew. Chem., Int. Ed.* **2013**, *52*, 5552.

(30) Hong, Y.; Blackman, N. M. K.; Kopp, N. D.; Sen, A.; Velegol, D. *Phys. Rev. Lett.* **2007**, *99*, 178103.

(31) Sengupta, S.; Dey, K. K.; Muddana, H. S.; Tabouillot, T.; Ibele, M. E.; Butler, P. J.; Sen, A. *J. Am. Chem. Soc.* **2013**, *135*, 1406.

(32) Saha, S.; Golestanian, R.; Ramaswamy, S. *Phys. Rev. E: Stat., Nonlinear, Soft Matter Phys.* **2014**, *89*, 062316.

(33) Dey, K. K.; Bhandari, S.; Bandyopadhyay, D.; Basu, S.; Chattopadhyay, A. *Small* **2013**, *9*, 1916.

(34) Cohen, J. A.; Golestanian, R. *Phys. Rev. Lett.* **2014**, *112*, 063802.

(35) Beck, J. S.; Vartuli, J. C.; Roth, W. J.; Leonowicz, M. E.; Kresge, C. T.; Schmitt, K. D.; Chu, C. T. W.; Olson, D. H.; Sheppard, E. W. *J. Am. Chem. Soc.* **1992**, *114*, 10834.

(36) Yanagisawa, T.; Shimizu, T.; Kuroda, K.; Kato, C. *Bull. Chem. Soc. Jpn.* **1990**, *63*, 988.

(37) Suzuki, N.; Jiang, X.; Radhakrishnan, L.; Takai, K.; Shimasaki, K.; Huang, Y.-T.; Miyamoto, N.; Yamauchi, Y. *Bull. Chem. Soc. Jpn.* **2011**, *84*, 812.

(38) Wu, K. C. W.; Yamauchi, Y. *J. Mater. Chem.* **2012**, *22*, 1251.

(39) Chiang, Y. D.; Lian, H. Y.; Leo, S. Y.; Wang, S. G.; Yamauchi, Y.; Wu, K. C. W. *J. Phys. Chem. C* **2011**, *115*, 13158.

(40) Wu, S.-H.; Mou, C.-Y.; Lin, H.-P. *Chem. Soc. Rev.* **2013**, *42*, 3862.

(41) Tang, F. Q.; Li, L. L.; Chen, D. *Adv. Mater.* **2012**, *24*, 1504.

(42) He, Q.; Shi, J. *J. Mater. Chem.* **2011**, *21*, 5845.

(43) Golestanian, R.; Liverpool, T. B.; Ajdari, A. *Phys. Rev. Lett.* **2005**, *94*, 220801.

(44) Popescu, M. N.; Dietrich, S.; Tasinkevych, M.; Ralston, J. *Eur. Phys. J. E* **2010**, *31*, 351.

(45) Ebbens, S.; Gregory, D. A.; Dunderdale, G.; Howse, J. R.; Ibrahim, Y.; Liverpool, T. B.; Golestanian, R. *EPL (Europhys. Lett.)* **2014**, *106*, 58003.

(46) Brown, A.; Poon, W. *Soft Matter* **2014**, *10*, 4016.

(47) Möller, K.; Kobler, J.; Bein, T. *Adv. Funct. Mater.* **2007**, *17*, 605.

(48) Kobler, J.; Möller, K.; Bein, T. *ACS Nano* **2008**, *2*, 791.

(49) Zhang, Q.; Wang, X.; Li, P.-Z.; Nguyen, K. T.; Wang, X.-J.; Luo, Z.; Zhang, H.; Tan, N. S.; Zhao, Y. *Adv. Funct. Mater.* **2014**, *24*, 2450.

(50) Yamamoto, E.; Kitahara, M.; Tsumura, T.; Kuroda, K. *Chem. Mater.* **2014**, *26*, 2927.

(51) Yamamoto, K.; Imaoka, T.; Chun, W.-J.; Enoki, O.; Katoh, H.; Takenaga, M.; Sonoi, A. *Nat. Chem.* **2009**, *1*, 397.

(52) Maji, T.; Banerjee, S.; Biswas, M.; Mandal, T. K. *RSC Adv.* **2014**, *4*, 51745.

(53) Wang, S.; Wu, N. *Langmuir* **2014**, *30*, 3477.

(54) Restrepo-Perez, L.; Soler, L.; Martinez-Cisneros, C. S.; Sanchez, S.; Schmidt, O. G. *Lab Chip* **2014**, *14*, 1515.

(55) Chen, N.-T.; Cheng, S.-H.; Souris, J. S.; Chen, C.-T.; Mou, C.-Y.; Lo, L.-W. *J. Mater. Chem. B* **2013**, *1*, 3128.

(56) Li, Z.; Barnes, J. C.; Bosoy, A.; Stoddart, J. F.; Zink, J. I. *Chem. Soc. Rev.* **2012**, *41*, 2590.

(57) Ma, X.; Teh, C.; Zhang, Q.; Borah, P.; Choong, C.; Korzh, V.; Zhao, Y. *Antioxid. Redox Signaling* **2014**, *21*, 707.

(58) Luo, Z.; Ding, X.; Hu, Y.; Wu, S.; Xiang, Y.; Zeng, Y.; Zhang, B.; Yan, H.; Zhang, H.; Zhu, L.; Liu, J.; Li, J.; Cai, K.; Zhao, Y. *ACS Nano* **2013**, *7*, 10271.

(59) Yan, H.; Teh, C.; Sreejith, S.; Zhu, L.; Kwok, A.; Fang, W.; Ma, X.; Nguyen, K. T.; Korzh, V.; Zhao, Y. *Angew. Chem., Int. Ed.* **2012**, *51*, 8373.

DOI: 10.1021/jacs.5b02700
J. Am. Chem. Soc. 2015, 137, 4976−4979